

Short Communication

## The Effects of Pulsed Current Parameters on Porosity of Copper Prepared by Jet Electrodeposition

Hui Fan<sup>1,2,\*</sup>, Zhijing Li<sup>1</sup>, Yangpei Zhao<sup>3</sup>, Shankui Wang<sup>1</sup>, Sainan Cao<sup>2</sup>

<sup>1</sup> kewen college, School of Mechanical and Electrical Engineering, Jiangsu Normal University, Xuzhou, 221116, China

<sup>2</sup> Jiangsu Key Laboratory of 3D Printing Equipment and Application Technology, Nantong Institute of Technology, Nantong, 226002, China;

<sup>3</sup> Science department, Jiang su Jiangzhu Institute, Xuzhou, 221116, China

\*E-mail: [xzfanhui@163.com](mailto:xzfanhui@163.com)

Received: 12 January 2019 / Accepted: 12 February 2019 / Published: 10 March 2019

---

Surface texturing has become an increasingly prevalent approach to improve the tribological properties of materials. The present work aims to study a novel texturing technology. A copper coating with a porous surface structure was directly prepared on stainless steel using a copper sulfate solution bath via high-speed jet electrodeposition. A fine, uniform honeycomb structure with micron sized pores can be achieved using a pulsed current. The duty cycle, current density and current frequency of the pulsed current have a notable influence on the microstructure of the deposited surface. Decreasing the duty cycle and increasing the current density can help to achieve a homogeneous and fine porous surface. The mechanism for depositing a porous surface was discussed according to the roles of the current parameters in the formation of the coating microstructure.

---

**Keywords:** jet electrodeposition; porous structure; pulse current;

### 1. INTRODUCTION

Surface texturing is an effective means of improving the tribological properties of sliding contact elements and has been widely used in a range of engineering applications, including face seals, thrust bearings, prosthetic hip joints and piston rings [1-3]. Various methods have been used to fabricate textured surfaces, such as laser texturing [2,4], electro-discharge texturing [5], and maskless electrochemical texturing [6-8], among which laser surface texturing (LST) is widely known as the primary means for producing textured surfaces. Dong et al. [2] fabricated circular pits with diameters between 20 and 80  $\mu\text{m}$  on the surface of a circular sample. Hu et al. [3] and Ripoll et al. [9] fabricated patterns of micro-dimples on a Ti6Al4V alloy and coated them with a MoS<sub>2</sub> film to improve their friction

behaviour under dry sliding conditions. Guo and Ren [10-13] conducted a bionic wear-resistance test on soil samples for reference and prepared a bionic coupling surface consisting of a pitted silicon-nickel carbide substrate coated by combining laser engraving technology and electrodeposition. However, laser texturing currently faces the challenging problems of high energy consumption and complex processing procedures and auxiliary equipment. Substantial effort has been expended to develop new surface texturing methods for preparing anti-friction high-performance parts at low cost.

Over the last decade, jet electrodeposition has emerged as an additive micro-manufacturing method to produce high-performance coating materials and has attracted a substantial amount of attention in engineering applications [14, 15]. Jet electrodeposition was developed by Fletcher and Oliver [14] in 1972. Initially, this method was developed for use in the fast selective electroplating and fabrication of micro features by Dover et al. [16] and Kunieda et al. [17]. Jet electrodeposition employs general electrochemical principles and generates coating materials based on the metallic ions transferred from the anode to the cathode through an electrolytic solution. During the process, a high-speed electrolyte jet is impinged onto the cathode surface, which enables the current to pass from the anode (nozzle) to the cathode (work piece) [18-20]. As shown in Fig. 1, the current results in localized deposition only in the impinging zone, which is one of the key features of jet electrodeposition technology. On the other hand, since the electrolytic jet continuously supplies fresh electrolyte to the deposition area, it creates a hydrodynamic environment that forms a diffusion layer with a very small thickness [21], which results in deposition of metal ions onto the surface at a substantially higher rate than in conventional electroplating. Therefore, it also enables a much higher applied current density than in conventional electrodeposition and generates novel material structures. For instance, micro/nano-scale porous surface microstructures can be formed, which can evolve to act as pockets for storing lubricants, resulting in self-lubricating and wear-reducing effects between contact elements. In addition, this process is found to be rapid, simple, economical, cold working to avoid heating affects and flexible to changes in the surface morphology by adjusting the deposition conditions.

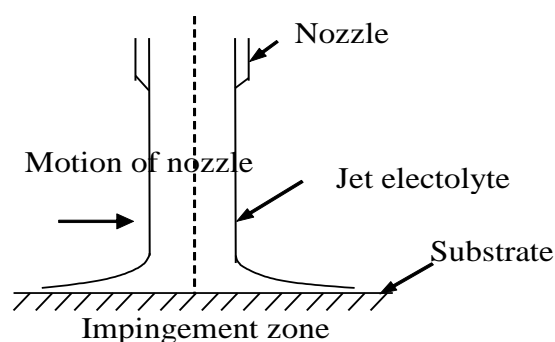


**Figure 1.** Schematic of the high-speed selective jet electrodeposition process

In previous studies, researchers have mainly employed jet electrodeposition for fast selective electroplating [22-24], because of the high current density, or for improving the wear resistance of coatings by means of crystal refinement or adding strengthening particles [25-27]. However, few studies have been performed on the micro/nano-porous-structure forming process and porous-structure generation mechanism. In this study, we constructed a copper coating with a uniform porous-structured

surface with pore sizes on the micron scale. The influential roles of the pulsed current parameters on the surface morphology and pore distribution are reported, and the porous-structure formation mechanism is discussed.

## 2. EXPERIMENTAL

The jet electrodeposition experimental setup (Fig. 2) consists mainly of an NC-controlled framework, nozzle and pulsed current power supply. A copper rod was placed in the anode chamber as the anode, and 30CrMnSi stainless steel, with a size of 100 mm×20 mm×2 mm, was used as the matrix material. The samples were polished using various grits of sandpaper and cleaned by soaking in distilled water and acetone for 5 minutes. The electrolyte composition and deposition process are shown in Table 1.

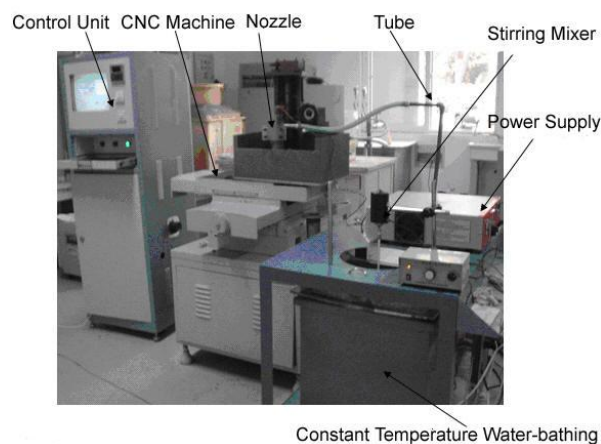


**Figure 2.** Diagram of the experimental setup for jet electrodeposition

**Table 1.** Electrolyte composition and deposition conditions

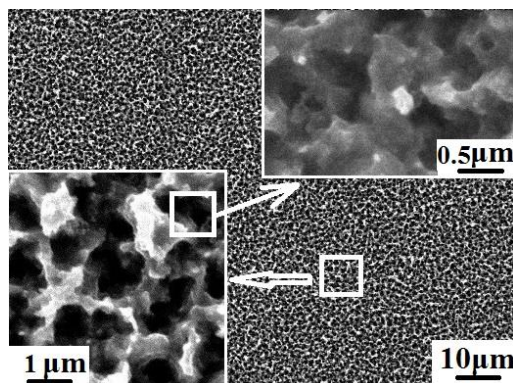
| Electrodeposition bath and process   | Composition and condition    |
|--------------------------------------|------------------------------|
| CuSO <sub>4</sub> ·5H <sub>2</sub> O | 250 (g/L)                    |
| H <sub>2</sub> SO <sub>4</sub>       | 50 (g/L)                     |
| pH                                   | 4                            |
| Current density                      | 200-600 (A/dm <sup>2</sup> ) |
| Duty cycle                           | 1:2-1:6                      |
| Temperature                          | 40±2 °C                      |
| Nozzle type                          | Rectangular 20 mm×1 mm       |
| Jet velocity                         | 10 m/s                       |
| Scan rate                            | 1000 mm/min                  |
| Deposition time                      | 30 min                       |

The morphologies and the crystallographic structures of the coatings were characterized using an LEO-1530 for field emission scanning electron microscopy (SEM). The microstructures were

examined by X-ray diffraction (XRD) spectrometry (D/max 2500VL/PC) operated at 40 kV and 300 mA with Cu K $\alpha$  radiation ( $\lambda= 1.5406 \text{ \AA}$ ) to determine the phase composition and the crystallite size.

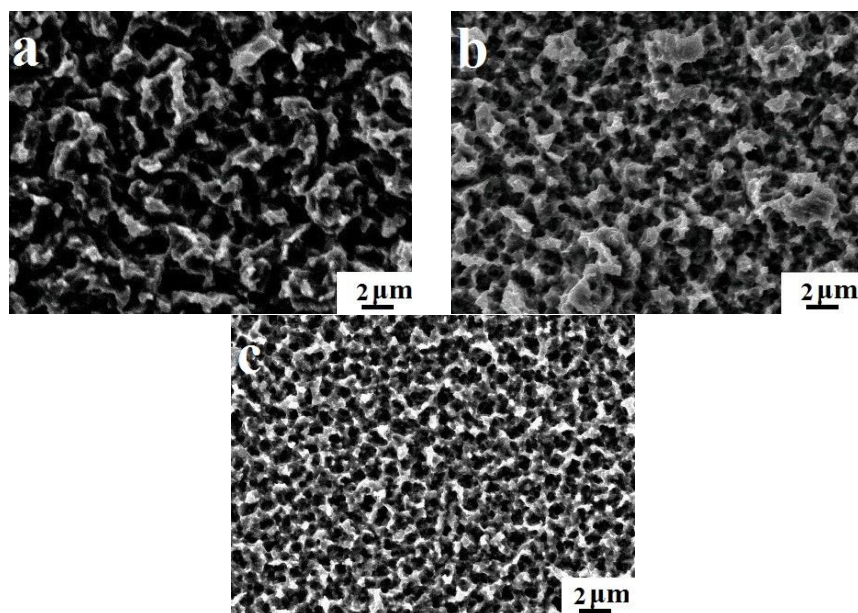
### 3. RESULTS AND DISCUSSION

Fig. 3 shows the micro-morphology of a surface deposited using a pulsed current duty cycle of 1:6. The surface appears uniform with fine porous structures and numerous microholes evenly distributed over the surface. To investigate the morphology of a single pore, a magnified image (bottom-left inset of Fig. 3) is presented. This image shows that a large number of small particles, with a size of 1  $\mu\text{m}$ , are arranged in a close and orderly manner on the deposited layer, forming a micro-porous honeycomb-like pattern. A number of smaller pores, much less than 1  $\mu\text{m}$  in size, also exist and are expected to be on the nanoscale (upper-right inset of Fig. 3). This indicates the existence of micro/nano-porous structures, which can supply the appropriate environment for storing lubricants.



**Figure 3.** The morphology of a deposited surface at low and high magnification

#### 3.1 The influence of the duty cycle on the deposited microstructure



**Figure 4.** The cross-sectional morphologies of the coatings prepared with duty cycles of (a) 1:2, (b) 1:4, and (c) 1:6

Fig. 4 displays the cross-sectional morphological transformation of the coating, which transitions from a disordered, irregular distribution of large pores to a homogenous and fine micro-porous structure, prepared over the range of duty cycles from 1:1 to 1:6. With relatively large duty cycles of 1:2 or 1:3, the deposited surface remains coarse, and the formed pores are 3-4  $\mu\text{m}$  long and have a worm-like shape and disordered distribution (Fig. 4 a, b), with a relatively low porosity of approximately 55%. As the duty cycle decreases to 1:6, more pores appear, and the shape of the pores becomes more rounded and regular, with a relatively high porosity of approximately 71%. Moreover, the porous structures are distributed more homogeneously, indicating that the porous morphology has significantly improved. This improvement is thought to be closely related to the change of the pulsed duty cycle because if a lower duty cycle is applied, then the pulse interval is longer, and more metal ions will be transported to the cathode to replace those consumed during the previous pulse [11]. This effect improves ion-concentration restoration and promotes more seeds for nucleation.

Additionally, the removal of the electric field during the pulse interval prevents single crystals from growing. Based on synergistic effects, more nucleation encourages the generation of refined and homogenous microstructures. However, a duty cycle less than 1:6 is not appropriate because a duty cycle that is too small could slow down the growth of the coating thickness and decrease the deposition efficiency. Therefore, the optimal duty cycle is 1:6, after consideration of the fine porous microstructures and deposition rates. Jiang et al. [27] prepared superhydrophobic surfaces on copper substrates by a common pulse electrodeposition process, with duty cycle ratios of 20%-80% in a lanthanum chloride electrolyte. Augustin et al. [28] and Gyawali et al. [29] produced copper thin films with textured surfaces on double zincated aluminium by using pulsed electrodeposition. Compared with these studies, jet pulsed electrodeposition can prepare textured copper and nickel coatings by a rapid facile one-step process, and the technology is much simpler.

### 3.2. The influence of the pulsed current on the deposited microstructure

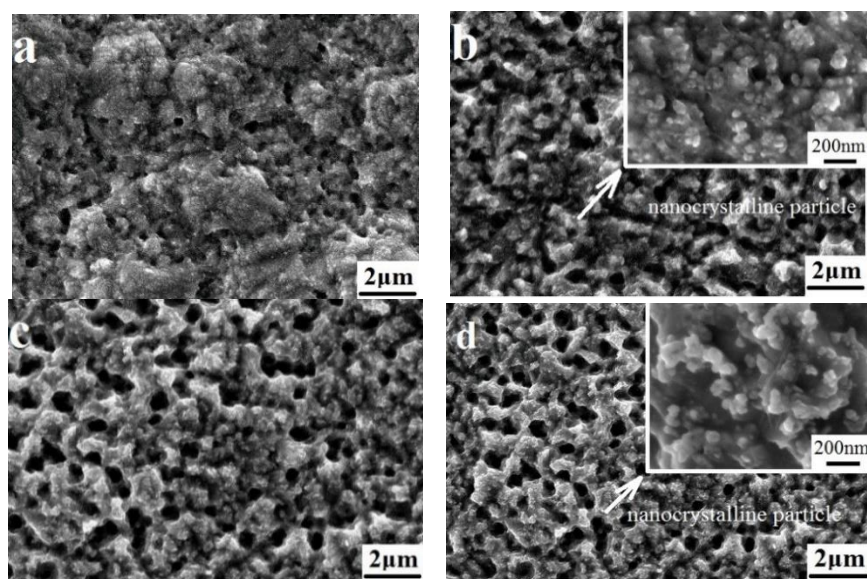


**Figure 5.** Microstructural morphology of the surface with current densities of (a) 200  $\text{A}/\text{dm}^2$  (b) 300  $\text{A}/\text{dm}^2$ , (c) 400  $\text{A}/\text{dm}^2$  and (d) 400  $\text{A}/\text{dm}^2$

Fig. 5 describes the cross-sectional morphological transformation of the coatings prepared with different current densities. As the current density increased from 200 A/dm<sup>2</sup> to 500 A/dm<sup>2</sup>, the grains that compose the deposited layer gradually became finer and more uniform. Simultaneously, there are an increasing number of pores that tend to be distributed more uniformly and densely over the surface, while individual pores become rounder and smaller. This change can be attributed to the increase in the current density, which results in a higher overpotential and leads to more nucleation. Magnified images of the coating microstructure is presented in the upper-right corners of Fig. 5 b and Fig. 5 d. It can be observed that the deposited layer is composed of nanocrystalline particles, most of which are between 30 and 50 nm.

On the other hand, according to X-ray diffraction analysis of samples prepared in the current density range of 200~500 A/dm<sup>2</sup>, as shown in Fig. 6 a, it can be seen that when the current density is 200~300 A/dm<sup>2</sup>, there is no obvious preferred orientation of the deposited layer. When the current density is greater than 300 A/dm<sup>2</sup>, the (111) crystal plane has the largest diffraction intensity, indicating it is the preferred crystal plan orientation. In previous studies, researchers [30,31] found that copper plating appeared to be highly preferentially oriented along the (111) crystal plane under high current densities [32], and the increase of the (111) crystal plane contributed to grain refinement. Tian et al. [33] also found that as the pulsed current density increased, the peak intensity of the (111) crystal plane increased and the coating grain size decreased. These published findings are in agreement with the current experimental results, indicating that the (111) crystal plane effects the grain refinement.

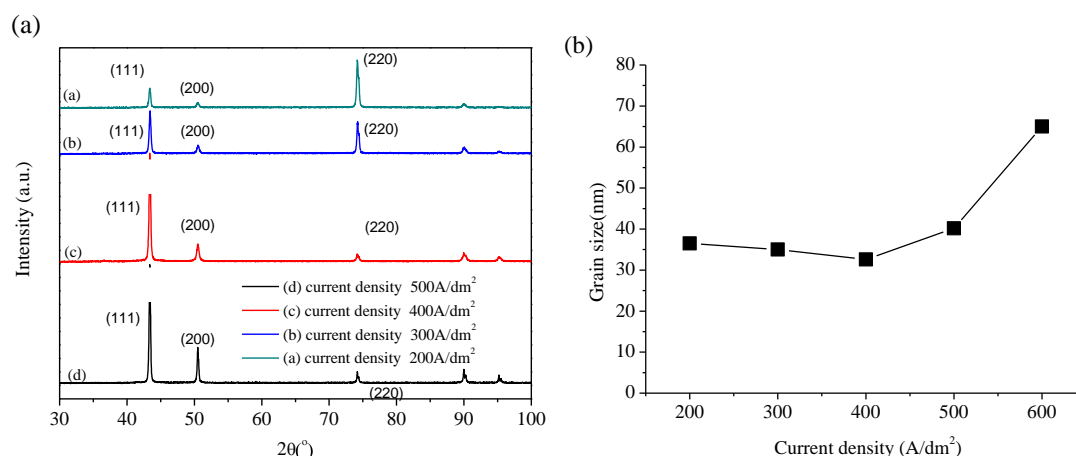


**Figure 6.** (a) XRD patterns and (b) coating grain sizes of different coatings prepared with different current densities

The trend for average grain size with changing current density is shown in Fig. 6 b over the current density range of 200~600 A/dm<sup>2</sup>. Overall, the grain size has no evident variation in the current density range of 200~400 A/dm<sup>2</sup>. Within this range, the average grain size decreases from 36 nm to 32 nm with increasing current density. In contrast, as the current density continues to increase beyond 400 A/dm<sup>2</sup>, the grain size of the deposited layer increases with increasing current density. When the current density has been increased to 600 A/dm<sup>2</sup>, the average grain size reaches its highest value, 65 nm. Therefore, the optimal current density, at which the smallest grain size can be obtained, is 400 A/dm<sup>2</sup>, and it is widely known that coating materials with fine grain sizes have good properties, such as their

mechanical performance [26, 34]. Zhu et al. [35] reduced the grain size of a Ni coating from 55 nm to 40 nm by means of friction-assisted electrodeposition. The reason for the reduced size was that mechanical friction can help breakdown crystals when they grow too fast, leading to the formation of numerous new screw dislocation defects, which facilitate crystal nucleation, increase the rate of nucleation, and eventually refine the grain size. Compared with these studies, jet electrodeposition can also refine the grain size of the coating by increasing the current density. This is because if a very high current density is applied, the rate of nucleation will greatly increase and the grains will be refined, correspondingly. In comparison, the jet electrodeposition method is easier to perform and more effective at refining the grains, achieving better mechanical performance.

The abovementioned deposited layer microstructure transition can be explained based on basic electrodeposition theory. In fact, an increase in the cathode current density can, accordingly, increase the cathode overpotential, which reduces the critical radius of nucleation and increases the probability of nucleation, so that a dense and refined microstructure in the deposited layer can be obtained. This effect illustrates the correlation between the increasing current density favouring the formation of dense and refined microstructures in the current density range of 200-400 A/dm<sup>2</sup>. However, if the current density exceeds 400 A/dm<sup>2</sup>, the mass transfer rate of the liquid phase cannot keep up with the consumption of metallic copper ions in the reduction reaction at the interface between the cathode and the solution. At this point, increasing the current density will only cause concentration polarization, and the grain growth rate will be higher than the formation rate of the crystal nuclei, resulting in an increased particle size as the current density increases.

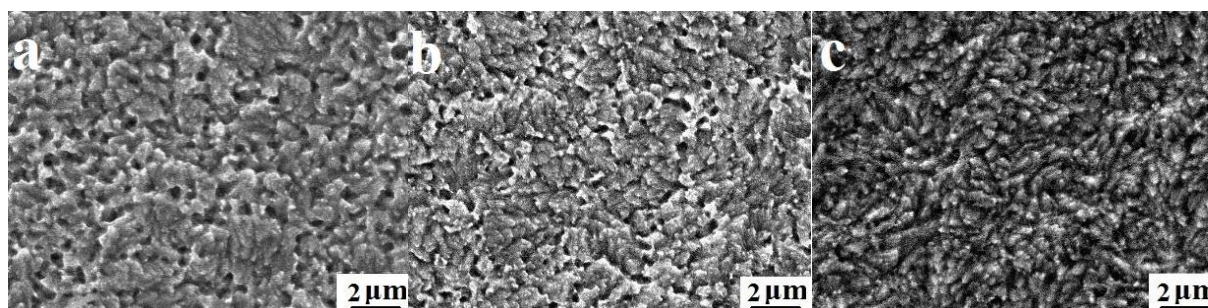
### 3.3. The influence of the pulsed current frequency on the deposited microstructure

Fig. 7 shows the cross-sectional morphological transformation of coatings prepared with different current frequencies; the parameters are shown in Table 2. As the pulse frequency increases, the microstructure is further refined with a consolidated compactness, and the amount of pores continues to decrease. As the pulse frequency varies from 5000 to 12,500 Hz, the structural morphology remains unchanged. When the pulse frequency rises to 12,500 Hz, the deposited surface becomes highly dense, and few pores can be identified. The above experimental observations reveal that the pulse current frequency influences the microstructure formation of the deposited layer. As the pulse frequency increases, the pulse width accordingly decreases, accompanied by shortening of the electric field action time. This variation is highly positive for the formation of crystal nuclei and, in contrast, restrains the growth of the grains. In addition, due to the presence of high-speed liquid mass transfer in electrolyte jet impingement, the metal ions consumed in the diffusion layer can be replenished over time, preventing the concentration polarization from increasing. Therefore, as the pulse current frequency increases, the compactness of the deposited coating increases and the porosity decreases. According to the literature [26], Xue et al. prepared high-quality composite electrodeposited coatings using traditional electrodeposition by increasing the pulse frequency. In comparison, jet electrodeposition can refine the grain size of the coating and produce uniform microstructures by varying the current frequency.

Moreover, jet electrodeposition has a better effect since the jet impingement can effectively enhance the role of the frequency in manipulating the deposited microstructure.

**Table 2.** Current density and pulsed current parameters

| Current density<br>(A/dm <sup>2</sup> ) | Pulse<br>frequency (Hz) | Pulse width<br>( $\mu$ s) | Pulse interval<br>( $\mu$ s) | Duty cycle |
|---|-------------------------|---------------------------|------------------------------|------------|
| 800                                     | 12,500                  | 20                        | 60                           | 1:4        |
|   | 5000                    | 50                        | 150                          |            |
|   | 2500                    | 100                       | 300                          |            |



**Figure 7.** Microstructural morphologies with pulsed current frequencies of (a) 2500 Hz, (b) 5000 Hz and (c) 12,500 Hz

#### 3.4. The porous structure formation process

Generally, electrocrystallization consists of nucleation and grain growth, which are included in the jet electrodeposition method. When the jet electrolyte impacts the cathode and is scanned across the surface, a vertical downward electrical field distribution is accordingly generated (Fig. 8 a, c). Nucleation occurs simultaneously against and perpendicular to the electric field. However, a high current density results in the formed grains growing preferentially against the electric field, gradually forming a multi-column ridge-like pattern (Fig. 8 c). Afterwards, because of the tip effect [18], the grains of the ridge tips will grow rapidly and expand towards both sides. When adjacent tip grains grow close enough to overlap, a porous mesh-like structure is formed (Fig. 8 b, d). Thus, it can be concluded that the electric field dominates the formation and distribution of the porous structures. Appropriate current parameters, especially for the duty cycle and current density, are key and capable of influencing the electric field distribution and further changing the size and pattern of the porous structures, as verified by the above experimental observations.

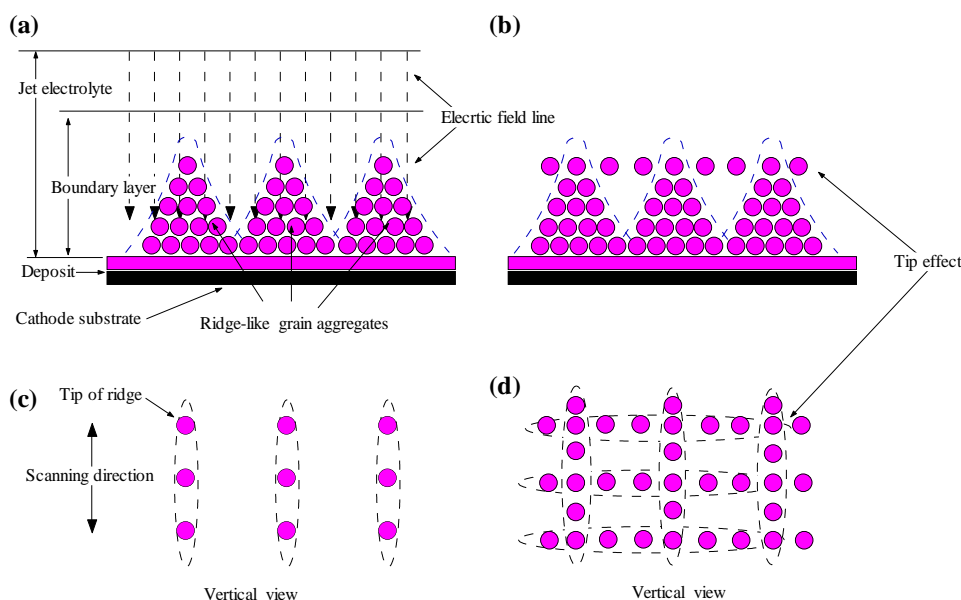


**Figure 8.** Schematic diagram of the porous structure formation by jet electrodeposition

#### 4. CONCLUSION

(1) A uniform deposited surface with micrometre sized pores was prepared by using jet electrodeposition. Additionally, micro/nanostructures were formed using a pulsed current.

(2) It was observed that the pulsed current parameters, including the duty cycle, current density and current frequency, influenced the coating microstructure. A decrease in the duty cycle and an increase in the current density can help achieve homogeneous and fine porous microstructures with refined nanocrystal grains, and the optimal parameters are a duty cycle of 1:6 and current density of 400 A/dm<sup>2</sup>.

(3) The mechanisms of porous surface formation using jet electrodeposition were explained, and the key to providing optimal current parameters is to apply an appropriate electric field to form a mesh-structure in the deposited coating.

#### ACKNOWLEDGEMENTS

This work was supported by the National Natural Science Foundation of China (51305178), Jiang Su Natural Science Foundation (BK20181473), Natural Science Foundation of Jiangsu Provincial University (17KJD460005), Nantong 3D printing laboratory funding project (2018KFKT09/CP12016002), College Students' innovation and entrepreneurship training program (201810320112Y)

#### References

1. X.H. Zheng, J. Tan, Q. Zhang, M. Wang and L.D Meng. *Surf. Coat. Technol.*, 311 (2017) 151.
2. D.R. Liu, Q. Zhang, Z.B. Qin, Q. Luo, Z. Wu and L. Liu. *Appl. Surf. Sci.*, 363 (2016) 161.
3. Z.E. Wu, Y.Q. Xing, P. Huang and L. Liu. *Surf Coat Technol.*, 309 (2017) 21.
4. K.Y. Zhang, J.G. Liu, W. Xiao and C.W. Yan. *Mater Lett.*, 193 (2017) 77.
5. D.R. Liu, Z. Wu, B Yan and B Shen, *Surf Eng.*, 33(2017) 877.

6. T. Darmanin, T.G. Elisabeth, A. Sonia and G. Frederic. *Adv. Mater.*, 25 (2013) 1378.
7. T. Ishizaki, Y. Masuda and M. Sakamoto. *Langmuir*, 27 (2011) 47808.
8. W. Tang, Y. Zhou and H. Zhu. *Appl Surf Sci.*, 273 (2013)199.
9. M.R. Ripoll, J. Brenner and B. Podgorni, *Tribol Let.t.*, 51(2013) 261.
10. D.Q. Zhao, X. Jiang and Y.X. Wang, *Appl Surf Sci.*, 457(2018)914.
11. M. Poorraeisi, A. Afshar, *Surf Coat Technol.*, 339(2018)199.
12. L. Zhang and C. Jing, *Electron. Process. Tech.*, 30 (2009) 230.
13. M. Alper, H. Kockar and M. Safak, *J. Alloys. Compd.*, 453 (2008) 15.
14. G.Y. Qiao, T.F. Jing, N. Wang, Y.W. Gao, X. Zhao, J.F Zhou and W. Wang. *Electrochim. Acta*, 51 (2005) 85.
15. H. Fan and Y. H. Huang, *Corros. Eng. Sci.Tech.*, 48 (2013) 48.
16. F.H. Su and K. Yao, *Acs. Appl. Mater. Interfaces*, 6 (2014) 8762.
17. G.F. Wang, L.D. Shen and L.M. Dou, *Int. J. Electrochem. Sci.*, 9 (2014) 3319.
18. H. Kima , J.G. Kimb , J.W. Parkc and C. N. Chu, *Precis. Eng.*, 51 (2018) 153.
19. M.S. Rajput, P. M. Pandey and S. Jha, *J. Manuf. Process.*, 17 (2015) 98.
20. F.F. Xia, W.C. Jia and C.Y. Ma, *Appl. Surf. Sci.*, 434 (2018) 228.
21. D. Z. Huang, L. D. Shen and J. S. Chen, *Trans. Indian. Inst. Met.*, 67 (2014) 351.
22. G. F. Wang, Z. J. Tian and Z. D. Liu, *Int. J. Electrochem. Sci.*, 10 (2015) 6844.
23. W. Jiang, L.D. Shen, Q.X. Wang, M.Z. Fan and Z.J. Tian, *J. Alloy. Compd.*, 762 (2018) 115.
24. L.D. Shen, Y.H. Wang and W. Jiang, *Corros. Eng. Sci. Technol.*, 52 (2017) 311.
25. X. Liu, L.D Shen, M.B. Qiu, Z.J. Tian, Y.H. Wang and K.L. Zhao, *Surf. Coat. Technol.*, 305 (2016) 231.
26. Z.M. Xue, W.N. Lei, Y.Q. Wang, H.F. Qian and Q.L. Li, *Surf. Coat. Technol.*, 325 (2017) 417.
27. S.Z. Jiang, Z.N. Guo, G.X. Liu, G.K. Gyimah, X.Y. Li, and H.S. Dong. *Materials*, 10 (2017) 1229.
28. A. Augustin, P Huilgol, K.R. Udupa and K.U. Bhat. *J. Mech. Behav. Biomed.*, 63 (2016) 352.
29. G. Gyawali, B. Joshi, K. Tripathi, S.H. Kim and S.W. Lee. *Surf. Eng.*, 31 (2015) 701.
30. X. Liu, L. D. Shen and M. B. Qiu, *Surf. Coat. Technol.*, 305 (2016) 231.
31. N. Piao, J. Chen, Y.W. Sun, Z.X. Xu, X.M. Chen and X. Han, *Electroplating & Pollution Control.*, 36 (2016) 4.
32. Y. Pan, S. Jiang, C.Y. Dai, T. Tang, Z.F. Zhou and Y.C. Zhou, *T. Nonferr. Met. Soc.*, 17 (2007) 770.
33. Z.J. Tian, D.S. Wang, G.F. Wang, L.D. Shen, Z.D. Liu and Y.H. Huang, *T. Nonferr. Met. Soc.*, 20 (2010) 1037.
34. B. Lu, Z.F. Hu, X.H. Wang and B.S. Xu, *Chinese. J. Nonferr. Met.*, 24 (2014) 137.
35. J. Zhu, Z.J. Tian, Z.D. Liu, L.D. Shen, Y.H. Huang and G.F. Wang, *J. South. China. Univ. Technol. Nat. Sci. Ed.*, 39 (2011) 92.